IEEE Access
Multidisciplinary ⋮ Rapid Review ⋮ Open Access Journal

Received January 27, 2020, accepted February 24, 2020, date of publication March 4, 2020, date of current version March 19, 2020.

Digital Object Identifier 10.1109/ACCESS.2020.2978436

Recognizing Hazard Perception in a Visual Blind Area Based on EEG Features

ZIZHENG GUO[1,2,3], YUFAN PAN[1,4], GUOZHEN ZHAO[5], JUN ZHANG[1,2], AND NI DONG[1,2,6]

[1]School of Transportation and Logistics, Southwest Jiaotong University, Chengdu 611756, China
[2]National United Engineering Laboratory of Integrated and Intelligent Transportation, Southwest Jiaotong University, Chengdu 611756, China
[3]National Engineering Laboratory of Intelligent Transportation Big Data Application Technology, Chengdu 611756, China
[4]School of Information Science and Technology, Southwest Jiaotong University, Chengdu 611756, China
[5]Key Laboratory of Behavioral Science, Institute of Psychology, Chinese Academy of Sciences, Beijing 100101, China
[6]Department of Civil and Environmental Engineering, University of Washington, Seattle, WA 98195, USA

Corresponding author: Zizheng Guo (guozizheng@swjtu.edu.cn)

This work was supported in part by the National Natural Science Foundation of China under Grant 51108390 and Grant 71601163, in part by the Science and Technology Program of Sichuan Province under Grant 2019YFG0043, and in part by the Science and Technology Program of China Railway under Grant 2018F024.

ABSTRACT Many potential hazards are encountered during daily driving in mixed traffic situations, and the anticipatory activity of a driver to a hazard is one of the key factors in many crashes. In a previous study using eye-tracking data, it was reliably recognized whether the eyes of a driver had become fixated or pursued hazard cues. A limitation of using eye-tracking data is that it cannot be identified whether the anticipatory activity of a driver to hazards has been activated. This study aimed to propose a method to recognize whether the psychological anticipation of a driver had been activated by a hazard cue using electroencephalogram (EEG) signals as input. Thirty-six drivers participated in a simulated driving task designed according to a standard psychological anticipatory study paradigm. Power spectral density (PSD) features were extracted from raw EEG data, and feature dimensions were reduced by principal component analysis (PCA). The results showed that when a driver detected a hazard cue, the alpha band immediately decreased, and the beta band increased approximately 300 ms after the cue appeared. Based on performance evaluation of the support vector machine (SVM), k-nearest neighbor (KNN) method, and linear discriminant analysis (LDA), SVM could detect the anticipatory activity of the driver to a potential hazard in a timely manner with an accuracy of 81%. The findings demonstrated that the hazard anticipatory activity of a driver could be recognized with EEG data as input.

INDEX TERMS Hazard perception, EEG, anticipatory activity, SVM.

I. INTRODUCTION

In daily driving, driver anticipation of on-road hazards that could cause a crash has been called hazard perception. It is claimed to be the only higher-order cognitive skill that reliably relates to the crash risk in drivers and plays a crucial role in crash likelihood prediction [1], [2]. Hazard perception is related to whether a driver can detect a potential hazard and prepare for it, and a traffic report revealed that approximately 40% of traffic accidents were caused by the lack of anticipation of potential hazards or unnoticed hazard cues [3]. Accelerating the learning process of hazard perception via assessment and training is one major strategy to improve traffic safety. Hazard perception can be viewed as the situation awareness of a driver for potentially dangerous incidents in the traffic environment. Typical conceptualization of situation awareness might help us more effectively design hazard-perception skill tests and training driving styles [4], [5]. Therefore, knowledge of this hazard-perception psychological process is cutting-edge research in the road safety field.

Due to the importance of hazard perception, many studies have focused on how to evaluate the hazard perception skills of drivers. These skills are mainly tested by video or driving simulator tests [6], [7]. In a typical video test, video clips recorded from the driver perspective are analyzed, and the responses when a hazard is detected are used to evaluate certain skills, such as manipulating a lever or pressing a response button to indicate the level of perceived risk [8]. The driving simulator test embeds potentially dangerous scenarios

The associate editor coordinating the review of this manuscript and approving it for publication was Zhaojun Li.

into the simulated driving task, which has a higher ecological validity than video tests [9], [10]. Furthermore, the hazard-perception skill has been regarded as an eligibility criterion of drivers, which is commonly known as the fitness to drive in recent years [11]. Applicants need to complete a computer-based hazard-perception test before being granted a valid driver's license in the United Kingdom and Australia [12]. Hazard perception is associated with perception and anticipation. Existing research effectively evaluated whether a driver perceived hazard cues but could not assess whether the anticipatory activity of the driver had been activated in preparation for potential hazards.

Anticipating a potential hazard is a cognitive process during which a person actively engages in a preparatory phase required for stimulus perception and executes specific actions after the appearance of a particular stimulus [13]. The psychological anticipation activity of a driver to coming events is activated by hazard cues. If a system could warn drivers when there is a potential hazard in cases when the driver psychological anticipation activity has not been activated, collision accidents could be more effectively avoided.

Studies have reported that electroencephalograms (EEGs) could represent anticipatory activities. The contingent negative variation (CNV), a slow, negative electrical brain wave, occurs in the interval between the presentation of cue and target stimuli in a cueing paradigm [14]. The cueing task is used as a classical experimental paradigm for studying the cognitive process of anticipation and has been widely investigated [15]. The CNV lasts from approximately 300 ms to several seconds with magnitudes up to 50 μV and has been linked to the preparatory process required for appropriate actions of coming events [16], [17]. In addition, the frequency domain of EEGs, which is more suitable for engineering applications, is also related to anticipation activities. The alpha band (7-13 Hz; alpha) is strongly correlated to the CNV in the interval between the cue and target stimuli [18]. A cue-induced alpha reflects attentional selection. Alpha decreases leading to liberalization of alpha when detecting a cue and anticipating a target in visual cueing tasks [19]. However, a warning stimulus would elicit a decrease in alpha [20], [21]. The beta band (13-30 Hz; beta) increases during the anticipation process, and beta oscillations are generally associated with motor preparation, which facilitates the action execution required based on the target stimulus [22], [23]. These findings indicated that the frequency domain information of EEGs could be used to detect the anticipation activities of drivers to potential hazards.

For identifying anticipation activities to a hazard in applications, a simulated driving experiment revealed that eye-tracking data could be used to reliably recognize whether the eyes of a driver had become fixated or were pursuing hazard cues [24]. This method can effectively provide a warning signal if the driver has not perceived cues. Generally, successful hazard perception should include detecting cues and preparing for executing evasive actions in terms of braking or steering [25]. A limitation of using eye-tracking data is that it cannot identify whether the anticipatory activity of the driver to hazards has been engaged. Since an EEG is a kind of physiological signal with a high temporal resolution [26], it could be used to represent the whole anticipatory activity process in CNV studies. As mentioned above, the EEG frequency showed a strong correlation with anticipatory activities. The results indicated that power features could be used to recognize whether the anticipatory activity of a driver to a hazard had been activated.

On this basis, a novel prediction method was proposed in this study that could estimate driver anticipatory activities to cues of potential hazards. This method could potentially advance the warning time from hazard onset to hazard cue detection in future driving assistance systems. We investigated the brain changing process during driver anticipatory activities upon detecting a hazard cue. The power spectral density (PSD) features of EEGs were used to recognize whether the anticipatory activity of driver to a potential hazard had been activated. We recorded simultaneous EEGs from 36 drivers performing a custom simulation driving task designed based on the standard S1-S2 paradigm, which is widely used to study anticipatory activities. The avoiding behavior of a driver before the appearance of the target stimulus was used to determine the label of each trial. PSD features were extracted from raw EEG data, and these features were fed into three widely used classifiers, including the support vector machine (SVM), k-nearest neighbor (KNN) and linear discriminant analysis (LDA). Finally, we compared the performance of these three classifiers to determine the best method to recognize driver anticipatory activities. As a result, the driver anticipatory activity to a potential hazard could be effectively recognized by SVM with the PSD features of EEG signals as input.

II. DATA DESCRIPTION

A. DRIVING SIMULATOR AND TASK

The experiment was conducted with a driving simulator consisting of a Logitech Driving Force G27 steering wheel with 2 pedals (throttle and brake pedals), a comfortable driving seat, and professional driving simulation software STISIM-DRIVE M100K [27]. The simulator provided a 60-degree vision from a driving perspective, as well as the flexibility to edit experimental scenarios. A 27-inch LCD display was used to visualize the driving task scenario, which was placed approximately 1 meter in front of the driver, with a resolution of 1920 $\times$ 1200 pixels and a refresh frequency of 60 Hz. The audio system consisted of a Sound Blaster X-FiTM sound card and a Dell A225 stereo system. These apparatuses provided a realistic driving environment.

Fig. 1 shows the design of the experiment in detail. The driving task scenario was a simulation of urban street driving, with two-way and two-lane roads. To isolate the effects of the cognitive load and avoid redundant actions that could result in EEG artifacts, there were no other moving vehicles except the experimental vehicle [28]. The task was designed according to the standard psychological paradigm of a S1-S2 task.

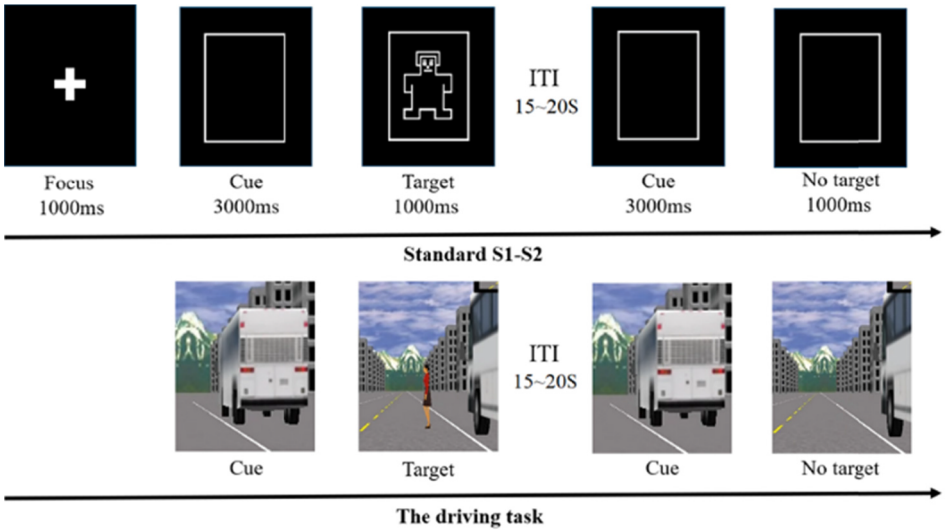

FIGURE 1. The design of the simulation driving task.

This paradigm has been widely used in psychological anticipatory studies [28]. In a standard S1-S2 task, each trial contends a cue stimulus (S1) and a target stimulus (S2). The anticipatory activity of subjects to the target stimulus is induced by S1, and the response to S2 is usually used to evaluate the anticipatory activity. In the driving task, participants were required to drive on the right side, and they remained at full throttle during driving (the simulator set the maximum speed of the vehicle to 45 km/h and the engine speed to 2200 rad/min). In each test trial, the vehicle would pass a bus station with a bus parked along the road side during driving, and a pedestrian would step onto the road when the vehicle passed the front end of the parked bus. The participant was required to steer to avoid a crash, then return to the right side and continue driving. In the trial, the parked bus represented the cue stimulus S1, and the pedestrian was the target stimulus S2. The interval between the pedestrian stepping onto the road and the parked bus appearing in the vision range of the driver was approximately 3 s at the design driving speed. After completing the test trial, another bus station would appear after 15∼20 s. There were 40 test trials in total for the whole task, and the probability of a pedestrian stepping onto the road was randomly set to 50% in all trials.

B. PARTICIPANTS AND EXPERIMENTAL PROCEDURE

Thirty-six fully licensed drivers participated in the driving experiment, including 22 males and 14 females. Their age ranged from 23 to 34 years old (a mean age of 26.6 years; standard deviation SD = 2.7 years). Their driving experience ranged from 1 to 10 years (a mean of 5.11 years; standard deviation = 2.3 years), and each participant had driven more than 5000 km in the past 6 months. All participants had normal or corrected normal vision, and none had any history of a neurological or psychiatric illness or required any medications or other forms of drugs that might influence the central nervous system. Drivers were recruited via online advertisements, and this study was approved by the Ethics Committee of the Institute of Psychology (CAS).

The participants were provided with information 24 hours before the test. They were well rested and were asked not to consume any caffeinated drinks such as coffee or tea and to arrive at the lab at 9:00 am. When participants arrived at the lab, the procedure was as follows:

1) The participants rested for 10 min to attain a resting state. At the same time, they were introduced to the experimental operations, and they signed informed consent forms thereafter.

2) After setting up the EEG electrodes, the participants were instructed to practice for 5 min and become familiar with the driving simulator and the special task.

3) In the formal experiment, the participants were required to drive with as few as necessary limb movements.

The entire experiment lasted approximately 15 min, and each participant received 100 CNY after completing the test.

C. DATA ACQUISITION

A 64-channel Neuroscan-SynAmps2 amplifier was used to record EEG signals, with 64 active electrodes attached to an electrode cap, which could record the required brain information for analysis. Electrode positions were mapped according to the standard international 10-20 system, and the left mastoid was used as the online reference for all channels. During the test, the impedance of all electrodes was controlled to be lower than 5k Ω, and the sampling rate of EEG data was set to 1000 Hz, while the electrodes were automatically filtered with a bandpass filter from 0 to 50 Hz.

Various driving parameters, such as steering angle and throttle and lane positions, were automatically recorded by software. The driving behavior and EEG data were synchronized through communication via a parallel port, and the driving simulator could transmit event codes to the EEG amplifier when the test trial was started. The sampling rate of driving behavior data was set to 50 Hz.

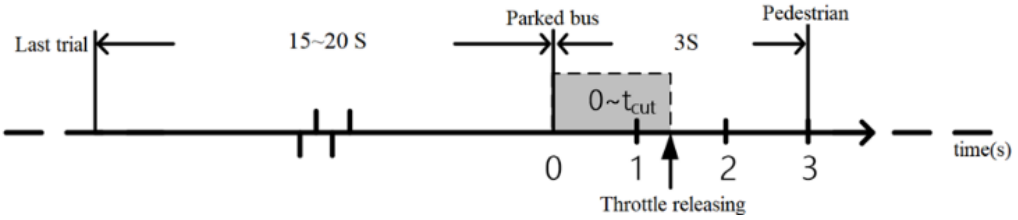

FIGURE 2. Schematic diagram of the trial.

III. METHODOLOGY

A. LABELING THE SAMPLES

One goal of this study is to use EEG data to recognize the anticipatory activity of a driver to a potential hazard upon detecting a hazard cue. In regard to the data, each test trial is a sample, and there are 1440 samples in total. Each sample label is determined based on the avoiding behavior before the appearance of the target stimulus.

When the anticipatory activity of the driver was activated by the cue in preparation for a potential hazard, specific driving behaviors would occur, such as reducing the speed [29]. In this study, the anticipatory avoiding action of releasing the throttle was used to label the sample. A schematic diagram of a trial is shown in Fig. 2, and the sample is labeled according to equation (1): The time when the parked bus appears in the vision range of the driver is set as 0 points, and the pedestrian steps onto the road within 3 s with a probability of 50%. If the driver releases the throttle pedal up to 95% and maintains that position until the target appears at 3 s, then this sample is labeled as a trial with anticipatory activity (WA). The sample label is 1. The point at which the throttle position is below 95% of its initial position is marked as t_{cut}, and the EEG data from 0 to t_{cut} is extracted for later analysis. On the other hand, if the driver does not release the throttle pedal within 3 s, this sample is labeled as a trial without anticipatory activity (WOA), and the sample label is -1. Hence, the label database is $Y = \{y_i\}, for\ i = 1, 2, \ldots, I$, and I is the number of samples.

$$f(n) = \begin{cases} 1, & the\ driver\ released\ throttle \\ -1, & others \end{cases} \tag{1}$$

B. EEG FEATURE EXTRACTION

1) ARTIFACT REMOVAL

The original EEG data may contain many artifacts, including electromyograms (EMGs) and electrooculograms (EOGs). First, the raw EEG data were filtered with a bandpass filter (from 0.1-30 Hz) to remove any linear trends and EMG artifacts. Then, the data were loaded in EEGLAB, and independent component analysis (ICA) was performed to decompose the data into independent components. EMG and EOG components were manually removed, and the remaining components constituted the artifact-free EEG data. Moreover, we referenced the average data of all electrodes.

2) FEATURE EXTRACTION AND DIMENSION REDUCTION

The EEG signal is the external representation of the brain, and its frequency and PSD characteristics are closely related to brain activity changes. According to previous studies, the PSDs of the alpha (α; 8-13 Hz) and beta (β; 13-30 Hz) bands change significantly due to anticipatory activities in the brain, which means that α and β can be adopted to recognize the anticipatory activity of a driver. The PSD is extracted from EEG data as follows:

For the WA trials, the EEG data of $[-\boldsymbol{T_{cut}}, \boldsymbol{T_{cut}}]$ were used to extract features, where $[-\boldsymbol{T_{cut}}, \mathbf{0}]$ was the baseline EEG, and $[\mathbf{0}, \boldsymbol{T_{cut}}]$ was the analyzed part. Features were extracted from the analyzed part minus the baseline, which means that the extracted PSD features represented the changes in EEG activity before and after the cue stimulus. For the WOA trials, the EEG range of $\left[-\mathbf{max}(\boldsymbol{T_{cut}}), \mathbf{max}(\boldsymbol{T_{cut}})\right]$ was used to extract features, where $\mathbf{max}(\boldsymbol{t_{cut}})$ is the maximum response time of a participant in all WA trials. Fig. 3 shows the process of EEG feature extraction. For each trial, a sliding Hamming window was adopted to divide the EEG data into segments with an overlap of 50%, and the length of the window was 200 ms. Fast Fourier transform (FFT) was implemented to transform the EEG data to the frequency domain. For segment data containing n data points, i.e., F(n), the amplitude density distribution function in the frequency domain is calculated as:

$$\boldsymbol{f_{FFT}(k)} = \begin{cases} \sum_{n=0}^{N-1} \boldsymbol{f(n)\, W_N^{kn}}, & \mathbf{0} \le \boldsymbol{k} \le \boldsymbol{N-1} \\ \mathbf{0}, & \boldsymbol{others} \end{cases} \tag{2}$$

where $\boldsymbol{W_n} = \mathbf{cos}\left(\frac{2\pi}{N}\right) - \boldsymbol{j}\mathbf{sin}\left(\frac{2\pi}{N}\right)$, $\boldsymbol{for\ N \approx n^2}$. According to the band of each PSD, the features of every Hamming window are calculated.

$$\begin{cases} \boldsymbol{PSD_\alpha} = \dfrac{\mathbf{1}}{\boldsymbol{f_\alpha}} \sum_{k \in f_\alpha} \| \boldsymbol{f_{FFT}(k)} \|^2 \\ \boldsymbol{PSD_\beta} = \dfrac{\mathbf{1}}{\boldsymbol{f_\beta}} \sum_{k \in f_\beta} \| \boldsymbol{f_{FFT}(k)} \|^2 \end{cases} \tag{3}$$

where $\boldsymbol{f_\alpha} = [\mathbf{8-13Hz}]$ $\boldsymbol{and}$ $\boldsymbol{f_\beta} = [\mathbf{13-30\ Hz}]$. Then, the original PSD features extracted from the baseline and analyzed EEGs were averaged, and specific PSD features were obtained by using the averaged original PSD features of the analyzed EEG minus the averaged original PSD features of the baseline EEG for each trial. In addition, we also adopted the ratio of $(\alpha + \beta)/\beta$ as a metric.

For each electrode, we can obtain 3 EEG PSD features. For q electrodes (q = 64 in this study) and I trials, the database is $\boldsymbol{X} = \{\boldsymbol{x_{il}}\}$, **for** $\boldsymbol{i} = \mathbf{1}, \mathbf{2}, \ldots, \boldsymbol{I}$ **and** $\boldsymbol{l} = \mathbf{1}, \mathbf{2}, \ldots, \mathbf{3}\boldsymbol{q}$.

Too many features as inputs would affect the running speed of the classification model and would also lead to data dimension disasters. To eliminate the data redundancy of the 3q column features, principal component analysis (PCA)

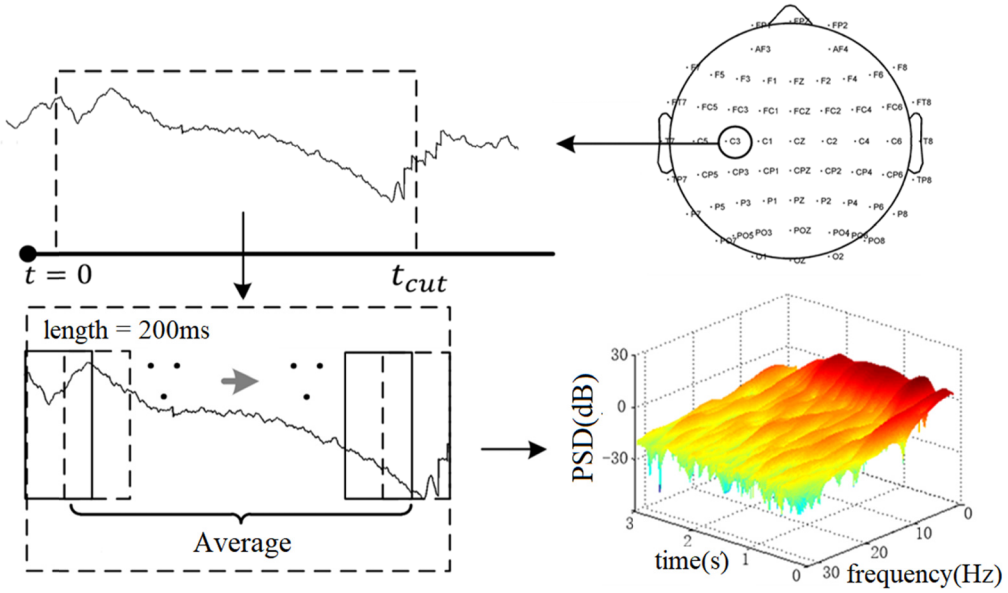

FIGURE 3. The process of EEG feature extraction.

was applied to compress the EEG features. PCA is a widely used dimension reduction method that converts similar data into linearly unrelated data by orthogonal transformation and converts multiple features into a few comprehensive features. In this study, L items with a cumulative contribution rate higher than 85% were selected as inputs of the classification model, and the feature database is $X' = \{x_{il}\}$, **for** $i = 1, 2, \ldots, I$, **and** $l = 1, 2, \ldots, L$.

3) THE CLASSIFIERS USED FOR COMPARISON

SVM, KNN and LDA were compared to recognize the hazard anticipatory activity of a driver in this study. SVM is a well-known binary linear classifier that establishes a hyperplane with certain exceptions and improves its discrimination ability by maximizing the margins. In the KNN method, the classifier labels samples are determined based on the similarity between samples in the training data. LDA is a technique that is used to describe the distinctive nature of two or more classes of objects by determining a linear combination of features.

Support Vector Machine (SVM). The mechanism of SVM consists of establishing the optimal classification hyperplane to adjust the classification requirements. The hyperplane can maximize the blank area on both sides of it while ensuring a high classification accuracy. It is suitable for high-dimensional and nonlinear classification with few samples. Given the database $\{x_i, y_i, i = 1, 2, \cdots, I\}$, *for* $x_i \in R^L$ *and* $y_i \in \{1, -1\}$, the optimal hyperplane is $w \cdot x + b = 0$. The problem of determining the optimal hyperplane can be transformed into the following nonlinear programming problems:

$$\begin{cases} min \dfrac{1}{2} \| w \|^2 \\ s.t. y_i (w \cdot x + b) \geq 1 \end{cases} \tag{4}$$

Using the Lagrange function to solve the optimization problem, the following is obtained:

$$L_1(w, b, a) = \frac{1}{2} \| w \|^2 + a(y(w \cdot x + b) - 1) \tag{5}$$

where a>0 is the Lagrange multiplier. The quadratic programming (QP) problem can be transformed into the following corresponding dual problems:

$$\begin{cases} maxQ(a) = \sum_{j=1}^{I} a_j - \frac{1}{2} \sum_{i=2}^{I} \sum_{j=1}^{I} a_i a_j y_i y_j (x_i \cdot x_j) \\ s.t. \sum_{j=1}^{I} a_i y_i = 0, a_j \geq 0, \text{ and } j = 1, 2, \ldots, I \end{cases} \tag{6}$$

The optimal solution is $a^* = (a_1^*, a_2^*, \ldots, a_I^*)^T$, and the optimal weights and bias are:

$$\begin{cases} w^* = \sum_{j=1}^{I} a_j^* y_j x_j \\ b^* = y_i - \sum_{j=1}^{1} y_i a_j^* (x_j \cdot x_i), j \in \{j | a_j^* > 0\} \end{cases} \tag{7}$$

Then, the optimal hyperplane is $w^* \cdot x + b^* = 0, s.t. w^* \in R^L$ *and* $b^* \in R$, and the best classification function is:

$$\begin{aligned} f(x) &= \text{sgn}\left(w^* \cdot x + b^*\right) \\ &= \text{sgn}\left\{ \left(\sum_{i=1}^{I} a_i^* y_i (x \cdot x_i) + b^* \right) \right\}, \quad x \in R^L \end{aligned} \tag{8}$$

When samples are linearly inseparable, the kernel function is used to map the samples to high-dimensional space ensuring that the samples are linearly divisible. The final classification function is:

$$f(\mathbf{x}) = \text{sgn}\left\{ \left(\sum_{i=1}^{I} a_i y_i k(x \cdot x_i) + b \right) \right\}, \quad \text{for } x \in R^L \tag{9}$$

where k $(x \cdot x_i)$ is the kernel function. In this study, the kernel function is the radial basis function (RBF).

$$\mathbf{k}(\mathbf{x} \cdot \mathbf{x_i}) = \exp\left(-\mathbf{g} \| x - \mathbf{x_i} \|^2 \right), \mathbf{g} > 0 \tag{10}$$

TABLE 1. Eight common similarity measures in KNN.

Similarity measures	Equation	Remarks
Euclidean distance	$\mathrm{d} = \sqrt{(x_i - x_j)(x_i - x_j)'}$	
City block distance	$\mathrm{d} = \sum_{l=1}^{L} \lvert x_{il} - x_{jl} \rvert$	
Chebychev distance	$\mathrm{d} = \max\{\lvert x_i - x_j \rvert\}$	
Hamming distance	$d = (\#(x_i \neq x_j)/n)$	The output of # (·) is 1 by XOR operation
Minkowski distance	$\mathrm{d} = \sqrt[p]{\sum_{l=1}^{L} \lvert x_i - x_j \rvert^p}$	C is the covariance matrix $\overline{x_i} = \frac{1}{L}\sum_{l=1}^{L} x_{il}$
Mahalanobis distance	$\mathrm{d} = \sqrt{(x_i - x_j)C^{-1}(x_i - x_j)'}$	
Correlation distance	$d = 1 - \frac{(x_i - \overline{x_i})(x_j - \overline{x_j})'}{\sqrt{(x_i - \overline{x_i})(x_i - \overline{x_i})'}\sqrt{(x_j - \overline{x_j})(x_j - \overline{x_j})'}}$	
Cosine distance	$d = (1 - \frac{x_i x_j'}{\sqrt{(x_i x_i')(x_j x_j')}})$	

where g is the RBF bandwidth, and the RBF has a good anti-interference ability to the sample noise.

K-Nearest Neighbor (KNN). KNN is a method based on mathematical statistics with a high accuracy for samples with unknown or non-normal distributions. For a given unknown sample, the main idea of KNN is to determine the k samples nearest to the unknown sample from training data and evaluate the unknown sample by counting the categories that appear the most out of these k samples. The model construction algorithm is described as follows:

1) Select a similarity measure and create a similarity matrix from the given training data.

2) Determine the k value and calculate the distance between the unknown sample and all training data.

3) Identify the k-nearest samples to the unknown sample.

4) Each category is counted, and the unknown sample belonging to the category with the highest frequency is predicted.

The similarity measure is a key factor in the performance of KNN. For any two samples $\boldsymbol{x_{iL}} = (\boldsymbol{x_{i1}}, \boldsymbol{x_{i2}}, \ldots, \boldsymbol{x_{iL}})$ *and* $\boldsymbol{x_{jL}} = (\boldsymbol{x_{j1}}, \boldsymbol{x_{j2}}, \ldots, \boldsymbol{x_{jL}})$, the distance between these two vectors is calculated according to the similarity measure, and there are 8 common similarity measures, which are summarized in Table 1.

Linear Discriminant Analysis (LDA). LDA is a classical pattern recognition algorithm, which was introduced by Belhumeur in 1996 in the fields of pattern recognition and artificial intelligence. To construct the LDA classifier, we assume that the WA and WOA samples in the training data belong to two different populations, G_1 and G_2, respectively, and the unknown sample x also belongs to either G_1 or G_2. The Mahalanobis distance between the unknown sample and the rest of the population is:

$$\mathbf{d}(\mathbf{x}\cdot\boldsymbol{G_i}) = \sqrt{(\boldsymbol{x}-\boldsymbol{\mu_i})' \sum_{\boldsymbol{i}}^{-1} (\boldsymbol{x}-\boldsymbol{\mu_i})}, \quad \mathbf{i} = \mathbf{1}, \mathbf{2} \tag{11}$$

where $\boldsymbol{\mu_i}$ are the mean-value vectors of the two populations, and $\boldsymbol{\Sigma}_\mathrm{i}$ are the covariance matrixes of the two populations. The discriminant function is:

$$\boldsymbol{f}(\mathbf{x}) = \frac{\mathbf{1}}{\mathbf{2}}[\boldsymbol{d^2}(\mathbf{x},\boldsymbol{G_1}) - \boldsymbol{d^2}(\boldsymbol{x},\boldsymbol{G_1}) - \boldsymbol{d^2}(\boldsymbol{x},\boldsymbol{G_2})] \tag{12}$$

If the covariance matrixes are equal, then $\Sigma_1 = \Sigma_2 = \Sigma$, and the discriminant function can be represented as:

$$f(\mathrm{x}) = 2(\mathrm{x} - \frac{\mu_1 + \mu_2}{2})^T \Sigma^{-1}(\mu_1 - \mu_2) \tag{13}$$

$$\begin{cases} if\ f\ (x) > 0, & x \in G_2, y = -1 \\ if\ f(x) < 0, & x \in G_1, y = 1 \\ if\ f\ (x) = 0, & x\ is\ unknown \end{cases} \tag{14}$$

For a given sample *x*, if $f(x) = -1$, the driver would not be prepared enough for the potential hazards, and if $f(x) = 1$, the driver would execute suitable actions in preparation for the potential hazards.

4) MODEL PERFORMANCE MEASUREMENT

For any unknown category sample x_i, the model can output one of four different results, namely, true positive (TP), which has an observed value of 1 and a predicted value of 1, false positive (FP), which has an observed value of -1 and an output of 1, true negative (TN), which has an observed value of -1 and an output of -1, and false negative (FN), which has an

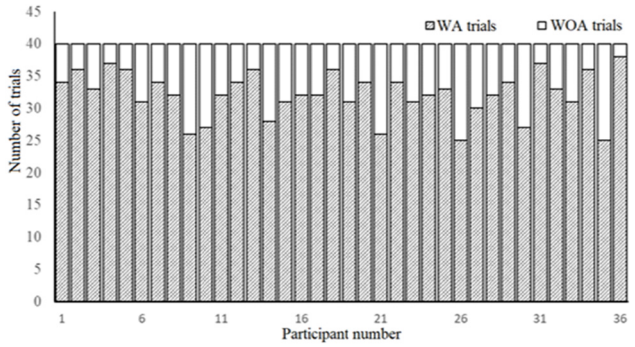

FIGURE 4. The number of anticipatory avoiding actions for each participant.

observed value of 1 and a predicted value of -1. The general accuracy (ACC), true positive rate (TPR) and true negative rate (TNR) were adopted to evaluate the performance of the above three classifiers, and these metrics were calculated as follows:

$$\mathrm{ACC} = \frac{TP + TN}{N_2} \times 100\% \tag{15}$$

$$\mathrm{TPR} = \frac{TP}{TP + FN} \times 100\% \tag{16}$$

$$\mathrm{TNR} = \frac{TN}{TN + FP} \times 100\% \tag{17}$$

where N_2 is the total number of test samples. In addition, the discriminability(d') and running time of each model were calculated in the performance comparison.

IV. EXPERIMENTAL RESULTS

A. DRIVING BEHAVIOR RESULTS

The driving behavior data are processed according to the method described in section III. There are 1440 samples in total, with 1156 WA samples and 284 WOA samples. The driving behavior distribution of each participant is shown in Fig. 4. For all participants, the average number of anticipatory avoiding actions is 32.04. Participant 26 performed the worst with 25 anticipatory avoiding actions, and participant 36 performed the best with 38 anticipatory avoiding actions. For the WA trials, the anticipatory avoiding action reaction time ranged from 316 to 733 ms. There were 592 WA trials in the first half of the experiments and 564 WA trials in the second half. This indicated that the drivers did not execute more anticipatory avoiding actions with increasing scenario familiarity. The average reaction time to the target stimulus for the WA trials was 487.12 (±86.33) ms, and that for the WOA trials was 532.62 (±82.05) ms, while the drivers in the WA trials performed quicker than those in the WOA trials ($t(718) = -5.83$, $p<0.01$), which indicated that the drivers were better prepared for the target stimuli in the WA trials. In addition, the Pearson correlation results revealed that there was no significant correlation between the driving experience and anticipatory avoiding actions ($p = 0.75$) in this study, which was also observed for the reaction time ($p = 0.24$). This would indicate that the tasks in the experiments measured the hazard perception of drivers at the cognitive functional level.

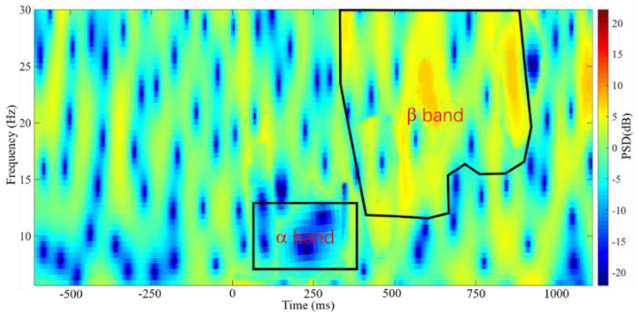

FIGURE 5. Changes in EEG when the driver detects the cue stimulus.

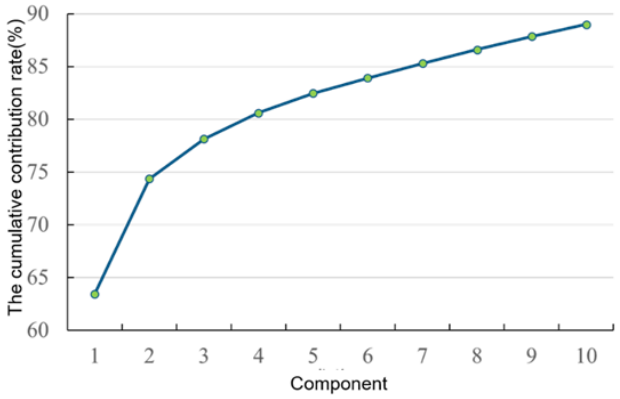

FIGURE 6. The cumulative contribution rate curve of PCA.

B. EEG ANALYSIS

Time-frequency analysis was conducted to examine the change process during EEG fluctuations. Fig. 5 shows the time-frequency map of the Cz electrode during a target trial. It is clear that when the driver detected the cue stimulus, the α band immediately decreased, and the β band became more active within approximately 300 ms. It was also confirmed that the PSD changes in the α and β bands could effectively represent the psychological anticipation activities of the drivers.

C. THE PCA RESULTS

Since there are 64 channels of EEG data, there are 192 original EEG features. PCA was applied to reduce the feature dimensions. As shown in Fig. 6, the cumulative contribution rate of the first seven principal components is higher than 85%, and these seven principal components of each sample were entered as input to the classifiers.

D. CLASSIFICATION RESULTS

1) DATA PARTITIONING

The database was divided into training and test data before the classification models were constructed. The training data were randomly selected, accounting for 70% of the WA and WOA samples. The remaining 30% of the samples constituted the test data. Table 2 summarizes the details of the training and test data. There are 1007 training samples in total,

TABLE 2. Details of the training and test data.

	WA (y=1)	WA (y=-1)	Total
Training data	809	198	1007
Test data	347	86	443

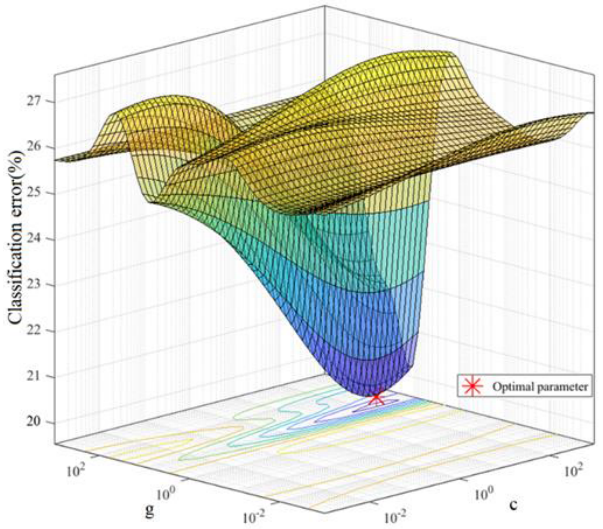

FIGURE 7. Parameter optimization of the SVM model.

of which 809 are WA samples and 198 are WOA samples. For the test data, there are 347 WA samples and 86 WOA samples, and the total number is 433. In this study, all classifiers were constructed with the same dataset.

2) RESULTS OF THE CLASSIFIERS

The performance of the SVM model is mainly affected by two parameters, the bandwidth g of the kernel function and the penalty parameter c. In this study, the SVM model are parameters optimized in MATLAB through default Bayesian optimization, and Fig. 7 shows the parameter optimization process. The optimal g value is 7.2, and the best c value is 11, with a smallest error of 18.7%.

The k neighbors and the similarity measure are the two parameters that affect the performance of KNN. In this study, we varied the k value and examined different similarity measures, and k was set to 10, 20, 30, 40, and 50. The similarity measures includes the Euclidean, city block, Chebychev, Hamming, Minkowski, Mahalanobis, correlation and cosine distances. Table 3 summarizes the performance of different combinations of k with the different similarity measures. When k was 20 with the similarity measure of the Mahalanobis distance, KNN attained the best performance with an error of 24.22%.

Fig. 8 shows the distance differences of all test samples to the two populations. The distance difference was calculated as the distance of each test sample to the WA population minus the distance of each test sample to the WOA population. In Fig. 8(a), the bars below the horizontal axis represent the WA test samples that have been correctly predicted,

TABLE 3. The performance for KNN with different parameters.

Similarity measures	k	Classification error rate (%)
Euclidean distance	20	24.25
City block distance	20	23.78
Chebychev distance	10	25.63
Hamming distance	10	25.40
Minkowski distance	20	24.24
Mahalanobis distance	20	24.22
Correlation distance	30	25.17
Cosine distance	30	24.45

TABLE 4. Confusion matrix of the SVM.

	Classified as WA	Classified as WOA
Observed WA	284	63
Observed WOA	19	67

TABLE 5. Confusion matrix of KNN.

	Classified as WA	Classified as WOA
Observed WA	260	87
Observed WOA	24	62

TABLE 6. Confusion matrix of LDA.

	Classified as WA	Classified as WOA
Observed WA	187	160
Observed WOA	46	40

and the bars above the horizontal axis in Fig. 8(b) represent the WOA test samples that have been correctly predicted. The performance of LDA is not good, and the ACC of all test samples is 52.42%. The results indicated that linear discrimination methods would not be suitable for distinguishing complex EEG features.

3) COMPARISON

To identify an effective classification model, three widely used classification models were compared in this study. All models were constructed and tested with the same training and test data, and default parameters were used in MATLAB 2018a. With 5-fold cross-validation, the classification accuracy of all test samples, including WA and WOA samples, was calculated to evaluate the models. The discriminability was adopted to evaluate the stability of the models. In addition, the running time was calculated to assess whether the models were suitable for online applications. Tables 4 to 6 summarize the confusion matrix of each model, and Table 7 summarizes the performance of the three models. As shown in Fig. 9, the SVM outperformed the other two classifiers, and it attained a classification accuracy of 81.24% with default settings, while discriminability exceeded 1.50. KNN produced a suboptimal result, but LDA was unable to distinguish the

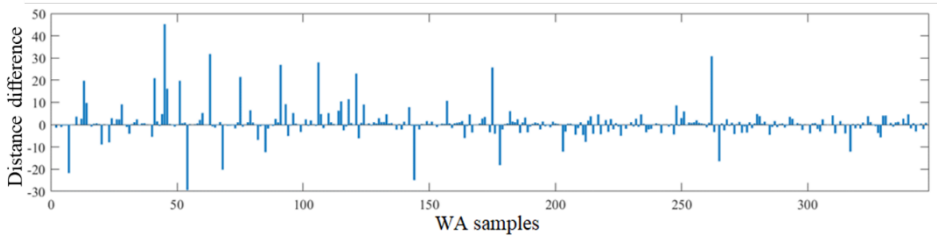

(a) The distance differences WA samples to two populations

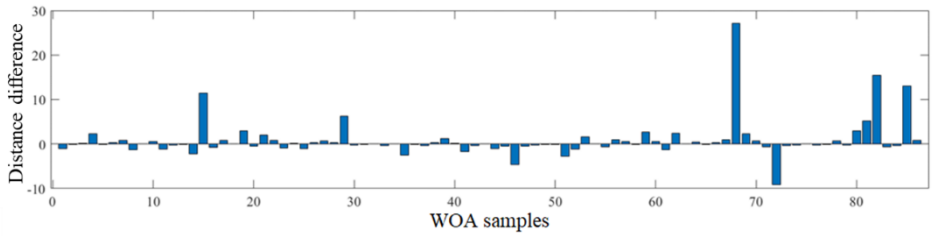

(b) The distance differences WOA samples to two populations

FIGURE 8. Distance differences of all test samples to the two populations.

TABLE 7. Comparison of the three classification models.

Model	ACC(%)	TPR(%)	TNR(%)	d'	Running time(ms)
SVM	81.06	82.84	77.91	1.68	117
KNN	74.36	74.92	72.09	1.19	102
LDA	52.42	53.02	46.51	0.11	60

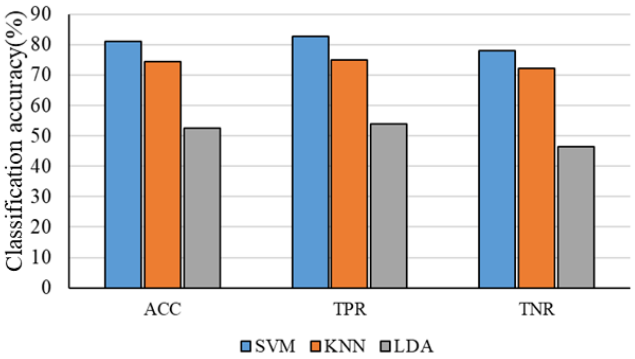

FIGURE 9. The performance of the three classifiers.

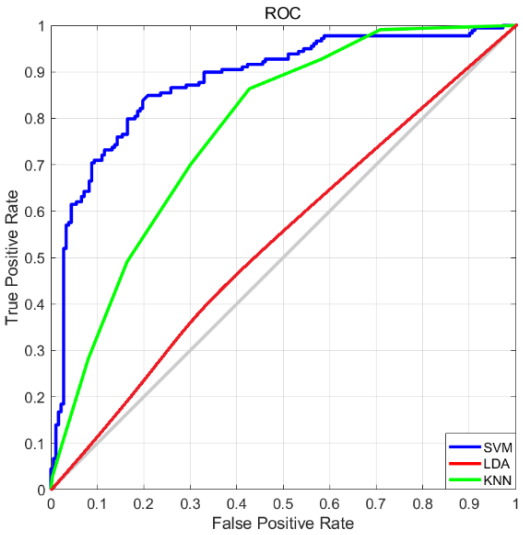

FIGURE 10. The ROC curve of the three classifiers.

different psychological anticipatory activities of the drivers. Moreover, Fig. 10 shows the receiver operating characteristic (ROC) curves of the three classifiers, and the area under the curve (AUC) is 0.81, 0.72 and 0.52. The results indicated that the SVM was more stable than the other two classifiers. Regarding the detection speed, although the running time of the SVM was slightly longer than those of KNN and LDA, it was only approximately 100 ms, which would have little effect on online applications.

With the optimal SVM parameters, we retrained and retested the model for validation. The average ACC was 80.24%, and the TPR was 84.47%, which was slightly higher than the ACC, but the TNR was slightly lower than the ACC at 78.92%, which indicated that the SVM model could better detect WA samples.

V. DISCUSSION AND CONCLUSION

The aim of this study was to propose a method that could be used to recognize whether a driver could anticipate a potential hazard upon detecting a hazard cue. We evaluated three classification models based on brain activity data and compared their performance. The data collected from simulated driving experiments (36 drivers) included those drivers who anticipated hazards, which was operationally assessed by the risk-avoiding actions executed before the target appeared. The experimental results revealed that the SVM was able to classify samples with an accuracy of 81% in approximately 100 ms. This finding demonstrates that the proposed method could be implemented to detect the hazard anticipatory activity of a driver.

In the current study, a new simulation driving task was proposed to investigate the hazard anticipatory activities of drivers. In contrast to the existing hazard-perception

test method, the task was designed according to the standard S1-S2 paradigm, and the effects of driving experience and cognitive load on the executed hazard anticipatory activities were eliminated by experimental control. This ensured that the psychological data collected in the experiments reflected the cognitive mechanism of hazard anticipation. The EEG PSD features represent the changes in brain activity of drivers before and after the hazard cue appeared. The time-frequency results represented the whole process during the hazard anticipatory activity. The main changes occurred in the α and β bands, namely, the α band decreased immediately, and the β band became more active immediately thereafter. Generally, the PSDs of the α and β bands have been used to estimate driver fatigue or vigilance, but studies have reported that these two bands are also related to anticipatory activities. The α band has been shown to play an important role in processing visual information [30]; a high α amplitude is associated with a reduced perceptual sensitivity [31], [32], and a pre-stimulus reduces the α amplitude in a previous anticipatory study [33], which means that the α band is inhibitory when the driver detects a visual hazard cue. In addition, the anticipatory activity is also related to the attention level. In the pedestrian crash scenario, the driver notices the parked bus, and this cue increases the level of vigilance when the driver anticipates a potential hazard, and β is an distinct vigilance index [34], [35].

To prevent accidents caused by the lack of hazard perception, researchers have developed a variety of driving assistance systems to help drivers in detecting hazards [36]–[39] or rely on visual intervention to attract the attention of drivers [40], [41]. For typical pedestrian collisions, the augmented reality (AR) technique has been used to detect the sudden appearance of a pedestrian and warn drivers [42], [43], or the car is stopped with an autonomous emergency braking system (AEB) when sensors detect a potential collision with a pedestrian [44], [45]. However, these systems do not perform well in emergency situations, and even the most intelligent level of the L3 autopilot system has failed in the 2019i-VISTA test. The explanation would be that the warning and AEB systems only start working after sensors have detected a pedestrian, and the time margin is insufficient to stop the car. These systems do not rely on cues of potential hazards, which results in visual blind areas. The proposed method makes up for the shortcomings of these systems. An ideal assistance system is a fusion of existing sensor-based systems and the proposed recognition method. By matching environmental information with the estimated anticipatory status of a driver via the brain-computer interface (BCI) system, the driver can be warned well in advance.

We have tried to recognize whether the anticipatory activity of a driver has been activated by a hazard cue with EEG PSD features, as opposed to using eye-tracking data [24]. The advantage of using EEG data is that the data represent the whole hazard-perception activity process. Using eye-tracking data, it can be recognized whether a driver detects a hazard cue, but it cannot be assessed whether the anticipation or vigilance level of the driver to the potential hazard has increased; in other words, detecting a hazard cue does not reflect how well a driver is prepared for a potential hazard in terms of physical and psychological aspects. The current study bridges this gap.

Three classification models were compared in this study, and the SVM outperformed the other two models in all measurements. However, it should be noted that all three models performed better in regard to the WA samples, which could be caused by the imbalance in sample proportion. In this study, the number of WA samples is approximately 3 times that of WOA samples, and more samples should be collected to further verify the proposed method in future research. The other limitation of this study is that we designed only one typical scenario in the experiments, but numerous different potential hazards are encountered in the mixed traffic environment of daily driving. More similar driving tasks will be designed in future studies, which would increase the applicability of the proposed method.

REFERENCES

[1] M. S. Horswill, "Hazard perception in driving," *Current Directions Psychol. Sci.*, vol. 25, no. 6, pp. 425–430, Dec. 2016.
[2] M. S. Horswill and F. P. Mckenna, "Drivers' hazard perception ability: Situation awareness on the road," in *A Cognitive Approach to Situation Awareness: Theory and Application*. 2004, pp. 155–175.
[3] *Global Status Report on Road Safety 2015*. World Health Org., Geneva, Switzerland, 2015.
[4] G. Li, S. E. Li, B. Cheng, and P. Green, "Estimation of driving style in naturalistic highway traffic using maneuver transition probabilities," *Transp. Res. C, Emerg. Technol.*, vol. 74, pp. 113–125, Jan. 2017.
[5] G. Li, Y. Wang, F. Zhu, X. Sui, N. Wang, X. Qu, and P. Green, "Drivers' visual scanning behavior at signalized and unsignalized intersections: A naturalistic driving study in China," *J. Saf. Res.*, vol. 71, pp. 219–229, Dec. 2019.
[6] C. T. Scialfa, M. C. Deschênes, J. Ference, J. Boone, M. S. Horswill, and M. Wetton, "A hazard perception test for novice drivers," *Accident Anal. Prevention*, vol. 43, no. 1, pp. 204–208, Jan. 2011.
[7] M. A. Wetton, M. S. Horswill, C. Hatherly, J. M. Wood, N. A. Pachana, and K. J. Anstey, "The development and validation of two complementary measures of drivers' hazard perception ability," *Accident Anal. Prevention*, vol. 42, no. 4, pp. 1232–1239, Jul. 2010.
[8] C. T. Scialfa, D. Borkenhagen, J. Lyon, and M. Deschênes, "A comparison of static and dynamic hazard perception tests," *Accident Anal. Prevention*, vol. 51, pp. 268–273, Mar. 2013.
[9] A. K. Pradhan, D. L. Fisher, and A. Pollatsek, "The effects of PC-based training on novice driversz' risk awareness in a driving simulator," in *Proc. 3rd Int. Driving Symp. Hum. Factors Driver Assessment, Training, Vehicle Design*, Iowa City, IA, USA, Oct. 2017, pp. 81–87.
[10] G. Underwood, D. Crundall, and P. Chapman, "Driving simulator validation with hazard perception," *Transp. Res. F, Traffic Psychol. Behav.*, vol. 14, no. 6, pp. 435–446, Nov. 2011.
[11] M. S. Horswill, "Improving fitness to drive: The case for hazard perception training," *Austral. Psychol.*, vol. 51, no. 3, pp. 173–181, May 2016.
[12] B. Liang and Y. Lin, "Using physiological and behavioral measurements in a picture-based road hazard perception experiment to classify risky and safe drivers," *Transp. Res. F, Traffic Psychol. Behav.*, vol. 58, pp. 93–105, Oct. 2018.
[13] W. G. Walter, R. Cooper, V. J. Aldridge, W. C. Mccallum, and A. L. Winter, "Contingent negative variation: An electric sign of sensori-motor association and expectancy in the human brain," *Nature*, vol. 203, no. 4943, pp. 380–384, Jul. 1964.
[14] J. J. Tecce, "Contingent negative variation (CNV) and psychological processes in man.," *Psychol. Bull.*, vol. 77, no. 2, pp. 73–108, 1972.
[15] A. W. K. Gaillard, "Effects of warning-signal modality on the contingent negative variation (CNV)," *Biol. Psychol.*, vol. 4, no. 2, pp. 139–153, Jun. 1976.

[16] W. Kirsch and E. Hennighausen, "ERP correlates of linear hand movements: Distance dependent changes," *Clin. Neurophysiol.*, vol. 121, no. 8, pp. 1285–1292, Aug. 2010.
[17] P. Kropp, A. Kiewitt, H. Göbel, P. Vetter, and W.-D. Gerber, "Reliability and stability of contingent negative variation," *Appl. Psychophysiol. Biofeedback*, vol. 25, no. 1, pp. 33–41, 2000.
[18] H. Mantanus, M. Timsit-Berthier, and B. Faucheux, "Is there a correlation between the phases of CNV and the power spectrum of the EEG?" *Revue D'electroencephalographie Neurophysiologie Clinique*, vol. 14, no. 2, pp. 97–102, 1984.
[19] C. Zhao, J. Guo, D. Li, Y. Tao, Y. Ding, H. Liu, and Y. Song, "Anticipatory alpha oscillation predicts attentional selection and hemodynamic response," *Hum. Brain Mapping*, pp. 3606–3619, May 2019.
[20] C. M. Gómez, E. Vaquero, D. López-Mendoza, J. González-Rosa, and M. Vázquez-Marrufo, "Reduction of EEG power during expectancy periods in humans," *Acta Neurobiologiae Experimentalis*, vol. 64, no. 2, pp. 143–152, 2004.
[21] M. Molnár, R. Csuhaj, Z. A. Gaál, B. Czigler, I. Ulbert, R. Boha, and I. Kondákor, "Spectral characteristics and linear–nonlinear synchronization changes of different EEG frequency bands during the CNV," *Psychophysiology*, vol. 45, no. 3, pp. 412–419, May 2008.
[22] N. Jenkinson and P. Brown, "New insights into the relationship between dopamine, beta oscillations and motor function," *Trends Neurosci.*, vol. 34, no. 12, pp. 611–618, Dec. 2011.
[23] T. Fischer, R. Langner, K. Diers, B. Brocke, and N. Birbaumer, "Temporospatial dynamics of event-related EEG beta activity during the initial contingent negative variation," *PLoS ONE*, vol. 5, no. 9, Sep. 2010, Art. no. e12514.
[24] E. Tafaj, T. C. Kübler, G. Kasneci, W. Rosenstiel, and M. Bogdan, "Online classification of eye tracking data for automated analysis of traffic hazard perception," in *Proc. Int. Conf. Artif. Neural Netw.*, Berlin, Germany, 2013, pp. 442–450.
[25] F. Sagberg and T. Bjørnskau, "Hazard perception and driving experience among novice drivers," *Accident Anal. Prevention*, vol. 38, no. 2, pp. 407–414, Mar. 2006.
[26] P. R. Davidson, R. D. Jones, and M. T. R. Peiris, "EEG-based lapse detection with high temporal resolution," *IEEE Trans. Biomed. Eng.*, vol. 54, no. 5, pp. 832–839, May 2007.
[27] S. Y. Choi, D. H. Yoo, and J. S. Lee, "Usefulness of the driveABLE cognitive assessment in predicting the driving risk factor of stroke patients," *J. Phys. Therapy Sci.*, vol. 27, no. 10, pp. 3133–3135, 2015.
[28] S. W. Savage, D. D. Potter, and B. W. Tatler, "Does preoccupation impair hazard perception? A simultaneous EEG and eye tracking study," *Transp. Res. F, Traffic Psychol. Behav.*, vol. 17, pp. 52–62, Feb. 2013.
[29] J. Edquist, C. M. Rudin-Brown, and M. G. Lenné, "Speed choice and hazard perception in complex urban road environments with and without on-street parking," in *Proc. Austral. Road Saf. Res., Educ. Policing Conf.*, Perth, WA, Australia, 2011, pp. 1–8.
[30] S. Nelli, S. Itthipuripat, R. Srinivasan, and J. T. Serences, "Fluctuations in instantaneous frequency predict alpha amplitude during visual perception," *Nature Commun.*, vol. 8, no. 1, pp. 1–12, Dec. 2017.
[31] N. Busch, J. Dubois, and R. VanRullen, "The phase of ongoing EEG oscillations predicts visual perception," *J. Vis.*, vol. 9, no. 8, p. 737, Sep. 2010.
[32] K. E. Mathewson, G. Gratton, M. Fabiani, D. M. Beck, and T. Ro, "To see or not to see: Prestimulus phase predicts visual awareness," *J. Neurosci.*, vol. 29, no. 9, pp. 2725–2732, Mar. 2009.
[33] G. Rohenkohl and A. C. Nobre, "Alpha oscillations related to anticipatory attention follow temporal expectations," *J. Neurosci.*, vol. 31, no. 40, pp. 14076–14084, Oct. 2011.
[34] O. Dehzangi and C. Williams, "Towards multi-modal wearable driver monitoring: Impact of road condition on driver distraction," in *Proc. IEEE 12th Int. Conf. Wearable Implant. Body Sensor Netw. (BSN)*, Cambridge, MA, USA, Jun. 2015, pp. 1–6.
[35] M. S. Haque, "Detection of a Driver's Eye Blinks and Brain Wave in Different Scenarios by EEG to Measure Drowsiness," M.S. thesis, Dept. Comput. Sci., San Diego State Univ., San Diego, CA, USA, 2015.
[36] G. Li, Y. Yang, and X. Qu, "Deep learning approaches on pedestrian detection in hazy weather," *IEEE Trans. Ind. Electron.*, to be published, doi: 10.1109/TIE.2019.2945295.
[37] G. Li, S. E. Li, R. Zou, Y. Liao, and B. Cheng, "Detection of road traffic participants using cost-effective arrayed ultrasonic sensors in low-speed traffic situations," *Mech. Syst. Signal Process.*, vol. 132, pp. 535–545, Oct. 2019.
[38] S. E. Li, G. Li, J. Yu, C. Liu, B. Cheng, J. Wang, and K. Li, "Kalman filter-based tracking of moving objects using linear ultrasonic sensor array for road vehicles," *Mech. Syst. Signal Process.*, vol. 98, pp. 173–189, Jan. 2018.
[39] X. Zeng, W. Ouyang, and X. Wang, "Multi-stage contextual deep learning for pedestrian detection," in *Proc. IEEE Int. Conf. Comput. Vis.*, Dec. 2013, pp. 121–128.
[40] X. Zhu, Z. Dai, F. Chen, X. Pan, and M. Xu, "Using the visual intervention influence of pavement marking for rutting mitigation—Part II: Visual intervention timing based on the finite element simulation," *Int. J. Pavement Eng.*, vol. 20, no. 5, pp. 573–584, Apr. 2017.
[41] G. Wu, F. Chen, X. Pan, M. Xu, and X. Zhu, "Using the visual intervention influence of pavement markings for rutting mitigation—Part I: Preliminary experiments and field tests," *Int. J. Pavement Eng.*, vol. 20, no. 6, pp. 734–746, 2019.
[42] H. Kim, J. L. Gabbard, A. M. Anon, and T. Misu, "Driver behavior and performance with augmented reality pedestrian collision warning: An outdoor user study," *IEEE Trans. Vis. Comput. Graphics*, vol. 24, no. 4, pp. 1515–1524, Apr. 2018.
[43] H. S. Park, "In-vehicle AR-HUD system to provide driving-safety information," *ETRI J.*, vol. 35, no. 6, pp. 1038–1047, Dec. 2013.
[44] L. Stark, M. Düring, S. Schoenawa, J. E. Maschke, and C. M. Do, "Quantifying vision zero: Crash avoidance in rural and motorway accident scenarios by combination of ACC, AEB, and LKS projected to german accident occurrence," *Traffic Injury Prevention*, vol. 20, no. sup1, pp. S126–S132, Aug. 2019.
[45] S. H. Haus, R. Sherony, and H. C. Gabler, "Estimated benefit of automated emergency braking systems for vehicle-pedestrian crashes in the united states," *Traffic Injury Prevention*, vol. 20, no. 1, pp. S171–S176, Aug. 2019.

ZIZHENG GUO received the B.S. degree in railway transportation, the M.S. degree in traffic safety, and the Ph.D. degree in traffic planning and management from Southwest Jiaotong University, Chengdu, China, in 2003, 2005, and 2009, respectively.

He was a Postdoctoral Fellow with the Institute of Psychology, Chinese Academy of Sciences, from 2011 to 2013, and was a Visiting Scholar at the University of Michigan, from 2013 to 2014. He is currently an Associate Professor with the Department of Transportation and Logistics, Southwest Jiaotong University.

YUFAN PAN received the B.S. degree in electronic information engineering from the University of Electronic Science and Technology of China, China, in 2014, and the M.S. degree in safety engineering from Southwest Jiaotong University, Chengdu, China, in 2018, where he is currently pursuing the Ph.D. degree with the Institute of Information Science and Technology.

His research interests include machine learning, traffic safety, and biomedical signal processing.

GUOZHEN ZHAO received the B.S. degree in industrial engineering from Tianjin University, China, in 2007, and the M.S. and Ph.D. degrees in industrial and systems engineering from the State University of New York at Buffalo, in 2009 and 2011, respectively.

He is currently an Assistant Professor with the Institute of Psychology, Chinese Academy of Sciences. His current research interests are mathematical modeling of human cognition and performance, human–computer interaction, emotion recognition, and augmented cognition.

JUN ZHANG received the B.S. degree in information science and technology and the M.S. degree in traffic planning and management from Southwest Jiaotong University, Chengdu, China, in 1998 and 2000, respectively.

His current research interests are traffic safety, human–computer interaction, and railway safety.

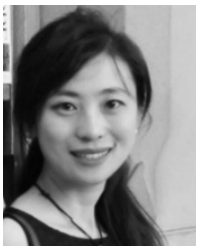

NI DONG received the B.S. degree in transportation engineering from the Changsha University of Science and Technology, China, in 2006, and the M.S. and Ph.D. degrees in transportation engineering from Central South University, China, in 2009 and 2015, respectively.

She was a Visiting Scholar at University of Washington, Seattle, from 2018 to 2020. She is currently an Assistant Professor with the Department of Transportation and Logistics, Southwest Jiaotong University. Her current research interests are statistical modeling of human mobility, human factor, traffic safety, and public health.